REPORT

QUANTUM OPTICS

Entanglement transport and a nanophotonic interface for atoms in optical tweezers

Tamara Đorđević[1]†, Polnop Samutpraphoot[1]†, Paloma L. Ocola[1]†, Hannes Bernien[2], Brandon Grinkemeyer[1], Ivana Dimitrova[1], Vladan Vuletić[3], Mikhail D. Lukin[1]*

The realization of an efficient quantum optical interface for multi-qubit systems is an outstanding challenge in science and engineering. Using two atoms in individually controlled optical tweezers coupled to a nanofabricated photonic crystal cavity, we demonstrate entanglement generation, fast nondestructive readout, and full quantum control of atomic qubits. The entangled state is verified in free space after being transported away from the cavity by encoding the qubits into long-lived states and using dynamical decoupling. Our approach bridges quantum operations at an optical link and in free space with a coherent one-way transport, potentially enabling an integrated optical interface for atomic quantum processors.

Systems of neutral atoms have recently emerged as a powerful platform for quantum simulations and quantum computation (*1*–*4*). Atom trapping, coherent control, and readout are enabled by optical beam arrays, whereas high-fidelity multi-qubit quantum gate operations are enabled either through tunneling (*5*) or coherent excitation into atomic Rydberg states (*6*). Many potential applications of these systems, from quantum networking to modular quantum computing, require a mechanism for transferring qubit states to optical photons without compromising the ability for multi-qubit control (*7*, *8*). Integration with a quantum optical interface, such as an optical cavity with switchable interactions, would enable the required atom-photon entanglement generation and distribution (*9*–*11*). A promising approach to achieve this is by spatially separating the cavity from the array and transporting selected atoms to and from the field as needed, preserving the coherence and scalability of atom array systems (Fig. 1A).

We demonstrate a system with a micrometer-size photonic crystal cavity (PCC) coupled to neutral atoms in movable optical tweezers that can perform high-fidelity single-qubit control and measurements as well as generate two-atom entanglement. Following the prior work that demonstrated coupling of atoms to photonic crystal structures (*12*–*14*), entangling atoms in macroscopic cavities (*15*, *16*), and coherently transporting atoms and ions in free space (*17*–*19*), we demonstrate PCC-mediated entanglement

[1]Department of Physics, Harvard University, Cambridge, MA 02138, USA. [2]Pritzker School of Molecular Engineering, University of Chicago, Chicago, IL 60637, USA. [3]Department of Physics and Research Laboratory of Electronics, Massachusetts Institute of Technology, Cambridge, MA 02139, USA.
*Corresponding author. Email: lukin@physics.harvard.edu
†These authors contributed equally to this work.

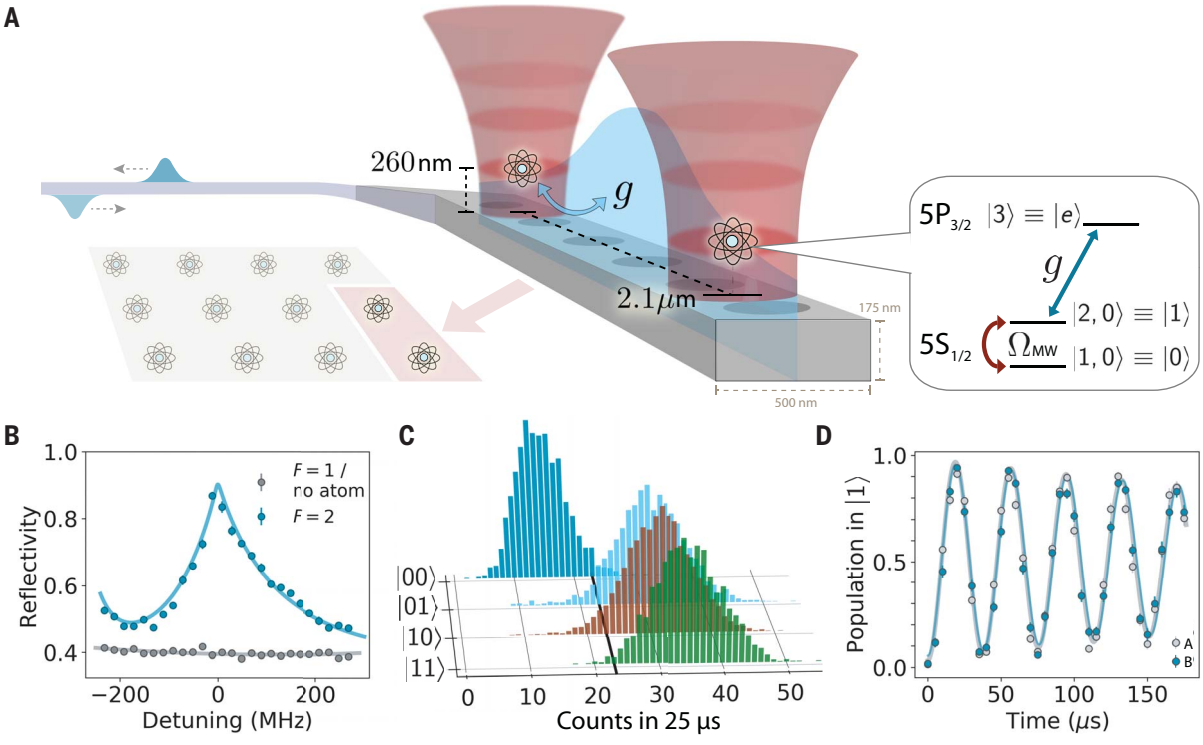

Fig. 1. Nanophotonic interface for atoms in tweezers. (**A**) A nanophotonic cavity could act as a photonic link for atom arrays serving as quantum information processors. Our system consists of two atoms in optical tweezers coupled to a fiber-linked cavity capable of a coherent one-way transport. (Inset) Atomic qubit states coupled by a microwave drive Ω_{MW}, with one coupled by the cavity field g to an excited state. (**B**) Cavity reflection spectrum for an atom in a strongly coupled state (blue) and an uncoupled state (gray), described by $(2g, \lambda, \kappa) = 2\pi \times (786, 6, 3800)$ MHz. (**C**) Readout of different two-qubit basis states by using the reflected photon counts. State $|00\rangle$ is distinguished from the others with fidelity $\mathcal{F} = 0.95(3)$. The atoms, cavity, and probe are on resonance. (**D**) Single-qubit Rabi oscillations in the cavity near-field showing preparation and coherent rotation with a π pulse fidelity $\mathcal{F}_\pi = 0.946(3)$.

generation that can be preserved and verified after transporting the atoms away from the cavity near-field. This is achieved by engineering a compact high-cooperativity photonic structure, establishing full quantum control in the near-field, encoding the qubits into field-insensitive states, and using dynamical decoupling sequences synchronized with the atomic transport.

In our experiments, two ^{87}Rb atoms were trapped in individually controlled optical tweezers and coupled to a PCC attached to a tapered optical fiber, enabling a low-loss photonic link out of the vacuum chamber (Fig. 1A) (*20*). The small cross-sectional area of the PCC (<0.1 μm^2) resulted in a small mode volume $V_m \sim 0.4\lambda^3$ that enabled high atom-photon cooperativity (*13*) and allowed for switching of the photon interactions by moving the atoms over ~1 μm in and out of the cavity near-field. Atoms at the PCC were trapped 260 nm above the surface by a standing wave created with the retro-reflection of the tweezer (*11*, *14*, *21*, *22*). Loading into the first lattice site of the standing wave was accompanied by a trapping potential deformation that resulted in an ~50% loading probability, which was increased to 80% by performing polarization gradient cooling during the transport to the PCC (*22*). [An efficiency above 90% without cooling during transport has been achieved with atoms initialized in the motional ground state (*21*).]

The cavity reflectivity strongly depends on the internal atomic state, with qubits encoded in $|0\rangle \equiv |F = 1, m_F = 0\rangle$ and $|1\rangle \equiv |F = 2, m_F = 0\rangle$. The PCC was tuned to be resonant with the $5S_{1/2}$, $F = 2 \rightarrow 5P_{3/2}$, $F' = 3$ optical transition and addresses all the m_F levels within these manifolds owing to the large cavity width κ. The reflection spectrum of a single atom is characterized by the extracted cooperativity $C = 4g^2/(\kappa\lambda) = 27(1)$ with a fit that accounts for thermal averaging (numbers in parentheses indicate 1 SD) (Fig. 1B) (*14*). When probed on resonance, the difference in reflectivity between an atom in the coupled $F = 2$ and uncoupled $F = 1$ manifold was used to perform a nondestructive single-shot readout. With two atoms, the uncoupled state $|00\rangle$ is distinguished from the other two-qubit states with high fidelity (Fig. 1C). This was used to determine the full two-atom state in all measurements at the PCC. For experiments in free space, readout was performed with state-selective push-out from the trap followed by fluorescence imaging. In both of these regimes, each pair of atoms was simultaneously prepared into $|0\rangle$ by using Raman-assisted state preparation (*22*) and addressed with a global microwave drive to perform single-qubit gates (Fig. 1D).

To coherently move the qubits from the near-field into free space, a millisecond coherence time was necessary. Choosing Zeeman-insensitive hyperfine sublevels as the qubit basis results in coherence times of $T'_2 = 2.1(1)$ ms and 9.7(8) ms in the near-field and free space, respectively, measured with a spin-echo pulse sequence (Fig. 2A). In the field-insensitive basis, the coherence is typically limited by the thermal motion that samples varying differential ac Stark shifts in the trap (*23*, *24*), and our measured T'_2 in free space is consistent with this model, given the trap parameters. The T'_2 at the PCC is likely further reduced by heating intrinsic to the near-field trapping geometry (*22*, *25*).

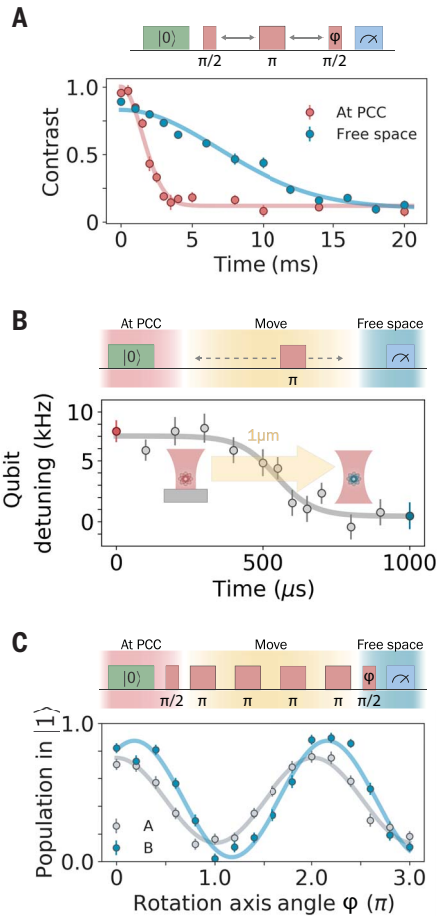

Fig. 2. Qubit coherence during the transport between the cavity and free space. (**A**) Measurement of the echo T'_2 for stationary traps at the PCC (red) and in free space (blue). (**B**) Changes in the trapping potential configuration during transport cause differences in the light shift and therefore qubit frequency, which can lead to additional dephasing. The gray line indicates fit to the programmed ramp. (**C**) Single-atom coherence for atoms in each trap (labeled "A" and "B") after transport measured in a Ramsey-type sequence. A four-pulse Carr-Purcell sequence symmetric with respect to the qubit frequency profile during transport was used to echo out the light shift variations.

Atomic coherence during transport is additionally affected by the change in differential ac Stark shift when moving between different trapping configurations. To observe this change, a detuned microwave π pulse was applied to single atoms at various times along the ~1-μm path from the PCC, where the measured population transfer is proportional to the instantaneous qubit frequency (*22*). From the resulting ramp profile in Fig. 2B, we obtained the minimal time of 650 μs to move from the PCC, limited by the mechanical response bandwidth of the scanning mirrors. Dephasing caused by fluctuations in the atom trajectory can be circumvented by using the Carr-Purcell decoupling pulse sequence (Fig. 2C) (*26*). This sequence was tested with the atom beginning in a superposition at the PCC and followed by $N \times \pi$ pulses along its transport, which performed better for an even N because of the symmetry of the ramp profile shown in Fig. 2B. The performance of the decoupling sequence was characterized separately in the two optical tweezers (trap A and trap B): For an optimal $N = 4$, an atom in trap B retains 0.88(5) of its initial coherence, limited by the move time and T'_2 (Fig. 2C). The lower contrast of 0.64(3) for an atom in trap A is ascribed to extra fluctuations in the scanning mirror, given that the traps are otherwise uniform. In addition to decoherence, each atom has an ~15% chance of being lost on the way out of the PCC, which is corrected for in the free space readout (*22*).

To generate an entangled state of atoms using the cavity, we performed a protocol known as "cavity carving" that projectively measures a classical superposition state while maintaining qubit indistinguishability (*27*, *28*), which can result in a maximally entangled Bell state (*16*, *29*). To implement the protocol, we initialized the atoms in $|00\rangle$, rotated by an angle θ to create the state

$$|\Psi_0\rangle = \cos^2\left(\frac{\theta}{2}\right)|00\rangle - \sin^2\left(\frac{\theta}{2}\right)|11\rangle - i\sin\left(\frac{\theta}{2}\right)\cos\left(\frac{\theta}{2}\right)(|01\rangle + |10\rangle) \quad (1)$$

We sent a weak coherent pulse into the cavity mode [$\bar{n} = 0.35$, chosen for negligible scattering error (*22*)] and conditioned on the detection of a reflected photon to project the state $|00\rangle$ out of the two-atom Hilbert space. The angle θ was chosen to maximize the overlap of the resulting state with $|\Psi^+\rangle = (|01\rangle + |10\rangle)/\sqrt{2}$, minimizing the population in $|11\rangle$ while accounting for the finite reflectivity of $|00\rangle$. For our system, the $|00\rangle$ reflectivity is already less than that of the other two-atom states (Fig. 1C). It was further reduced by an interferometer in the detection path and is ultimately limited by the interferometric stability (*22*). After the projection, an additional π/2 pulse was applied to

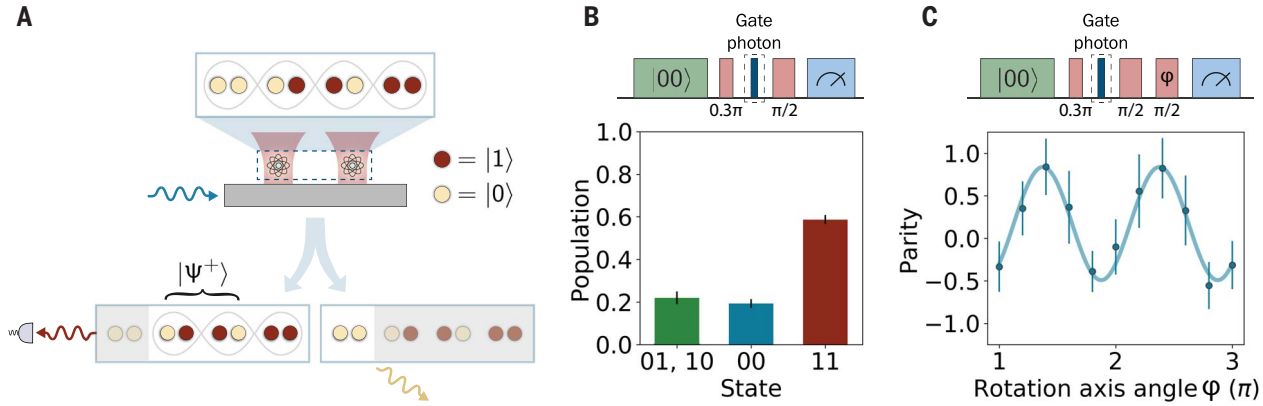

Fig. 3. Heralded entanglement at the cavity. (**A**) Protocol description. Postselection on a photon reflection from a superposition state carves out the $|00\rangle$ component, leaving the atoms predominantly in $|\Psi^+\rangle$. (**B**) Populations of the resulting state in different basis states. A π/2 pulse was applied before the measurement, converting the Bell state $|\Psi^+\rangle$ into $|\Phi^+\rangle$. $\{P_{11}, P_{00}\}$ is extracted {with, without} an additional global π pulse before cavity reflection readout. P_{01} and P_{10} cannot be distinguished. (**C**) Parity oscillations of the $|\Phi^+\rangle$ state after rotating over a varied axis ϕ, showing nonclassical correlations between the qubits in all bases. The coherence $\rho_{11,00}$ is extracted from the amplitude. The combined coherence and populations give a Bell state fidelity of $\mathcal{F} = 0.72(3)$.

rotate the Bell state $|\Psi^+\rangle$ into $|\Phi^+\rangle = (|00\rangle + |11\rangle)/\sqrt{2}$ for ease of characterization.

The entangled state was first characterized in situ by using the cavity reflection readout shown in Fig. 1C. The $|\Phi^+\rangle$ fidelity $\mathcal{F} = \langle\Phi^+|\rho|\Phi^+\rangle = \frac{1}{2}(\rho_{00,00} + \rho_{11,11}) + \mathrm{Re}(\rho_{00,11})$ was determined by measuring populations and extracting coherence from the parity oscillation contrast upon another π/2 rotation over different axes (*16*, *22*). Populations are plotted in Fig. 3B with $\mathcal{P} = P_{00} + P_{11} = 0.78(3)$; the imbalance between $|00\rangle$ and $|11\rangle$ is discussed and modeled in the supplementary materials (*22*). The parity oscillation in Fig. 3C corresponds to a coherence of $\rho_{11,00} = 0.33(2)$. These measurements give a fidelity of $\mathcal{F} = 0.72(3)$ and a concurrence bound of $\mathcal{C} \geq 0.46(5)$ (*22*). The major part of the error (24%) is accounted for by the chosen initial angle θ for our protocol, with an additional 4% from the initialization imperfections. Although our approach uses a single gate photon, heralding on repeated gates can improve the entanglement fidelity at the expense of the success probability (*16*).

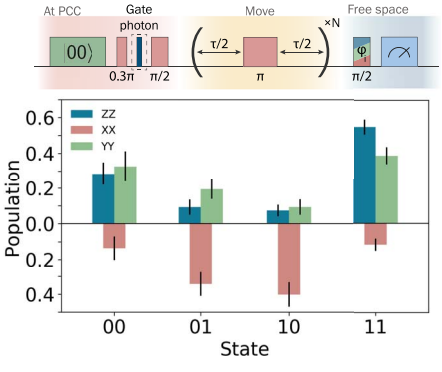

Fig. 4. Coherent transport of entangled atoms from the cavity to free space. After entangling the atoms at the cavity, the tweezers are moved away while applying dynamical decoupling. Free space readout in different bases after transport shows the remaining entanglement fidelity of $\mathcal{F} = 0.65(6)$, which is larger than the classical limit of 0.5.

Last, the entangled atoms were transported away from the cavity while applying decoupling pulses. The qubit state populations were measured in the *ZZ*, *XX*, and *YY* bases (Fig. 4), giving the population $\mathcal{P} = 0.78(6)$ and the coherence $\rho_{11,00} = 0.26(5)$, corrected for the atomic loss. This resulted in a fidelity of $\mathcal{F} = 0.65(6)$ and a lower bound to the concurrence of $\mathcal{C} \geq 0.35(11)$ [$\mathcal{F}_u = 0.52(5)$ and $\mathcal{C}_u \geq 0.04(10)$ without the readout correction]. Both $\mathcal{F} > 0.5$ and $\mathcal{C} > 0$ certify entanglement after transport at a 99% confidence level. The state fidelity is consistent with the decoherence observed for single atoms during transport (Fig. 2C), limited by atomic thermal motion and uncorrelated fluctuations in the programmed trajectories. The trajectory fluctuations can be reduced in the future by using an acousto-optic deflector (AOD) that would speed up the transport and enable atomic displacements of more than 100 μm, which is sufficient for high-fidelity Rydberg state control (*30*).

These results demonstrate that combining movable atoms in tweezers with nanophotonics constitutes a promising platform for the development of a quantum optical node for large-scale atomic quantum processors. If integrated with a free space atom array, our system could enable quantum teleportation of the atom array states to optical photons (*31*) or remote entanglement of arrays. This can be accomplished by using the demonstrated one-way transport, in which the atoms that are entangled with a photon at the PCC are then coherently moved to the free space array to interact through Rydberg gates. Extending our demonstration to a general-purpose quantum optical interface with a coherent two-way transport could enable feed-forward protocols such as quantum error correction by means of fast, high-fidelity quantum nondemolition cavity readout. Furthermore, with multiple atoms coupled to nanophotonic waveguides, entangled and arranged into arbitrary spatial configurations, important classes of many-particle quantum states can be created, such as atomic cluster or graph states (*32*), large-scale photonic Fock states (*33*), or Schrödinger cat states (*34*). Last, telecom transitions present in both alkaline-earth and alkali atoms (*35*, *36*) could extend atom-nanophotonic quantum networking to long distances, which is crucial for quantum communication and the scale-up of processing power (*8*).

REFERENCES AND NOTES

1. M. Saffman, T. G. Walker, K. Mølmer, *Rev. Mod. Phys.* **82**, 2313–2363 (2010).
2. S. Ebadi *et al.*, *Nature* **595**, 227–232 (2021).
3. P. Scholl *et al.*, *Nature* **595**, 233–238 (2021).
4. I. S. Madjarov *et al.*, *Nat. Phys.* **16**, 857–861 (2020).
5. A. M. Kaufman *et al.*, *Science* **345**, 306–309 (2014).
6. H. Levine *et al.*, *Phys. Rev. Lett.* **123**, 170503 (2019).
7. N. H. Nickerson, Y. Li, S. C. Benjamin, *Nat. Commun.* **4**, 1756 (2013).
8. C. Monroe *et al.*, *Phys. Rev. A* **89**, 022317 (2014).
9. T. Northup, R. Blatt, *Nat. Photonics* **8**, 356–363 (2014).
10. A. Reiserer, G. Rempe, *Rev. Mod. Phys.* **87**, 1379–1418 (2015).
11. T. G. Tiecke *et al.*, *Nature* **508**, 241–244 (2014).
12. J. D. Hood *et al.*, *Proc. Natl. Acad. Sci. U.S.A.* **113**, 10507–10512 (2016).
13. D. E. Chang, J. S. Douglas, A. González-Tudela, C.-L. Hung, H. J. Kimble, *Rev. Mod. Phys.* **90**, 031002 (2018).
14. P. Samutpraphoot *et al.*, *Phys. Rev. Lett.* **124**, 063602 (2020).
15. S. Welte, B. Hacker, S. Daiss, S. Ritter, G. Rempe, *Phys. Rev. X* **8**, 011018 (2018).
16. S. Welte, B. Hacker, S. Daiss, S. Ritter, G. Rempe, *Phys. Rev. Lett.* **118**, 210503 (2017).
17. J. Beugnon *et al.*, *Nat. Phys.* **3**, 696–699 (2007).
18. A. Lengwenus, J. Kruse, M. Schlosser, S. Tichelmann, G. Birkl, *Phys. Rev. Lett.* **105**, 170502 (2010).
19. J. M. Pino *et al.*, *Nature* **592**, 209–213 (2021).
20. T. G. Tiecke *et al.*, *Optica* **2**, 70 (2015).
21. J. D. Thompson *et al.*, *Science* **340**, 1202–1205 (2013).

22. Materials and methods are available as supplementary materials.
23. S. Kuhr *et al*., *Phys. Rev. A* **72**, 023406 (2005).
24. D. Reitz, C. Sayrin, R. Mitsch, P. Schneeweiss, A. Rauschenbeutel, *Phys. Rev. Lett.* **110**, 243603 (2013).
25. D. Hümmer, P. Schneeweiss, A. Rauschenbeutel, O. Romero-Isart, *Phys. Rev. X* **9**, 041034 (2019).
26. H. Y. Carr, E. M. Purcell, *Phys. Rev.* **94**, 630–638 (1954).
27. W. Chen *et al*., *Phys. Rev. Lett.* **115**, 250502 (2015).
28. G. Barontini, L. Hohmann, F. Haas, J. Estève, J. Reichel, *Science* **349**, 1317–1321 (2015).
29. A. S. Sørensen, K. Mølmer, *Phys. Rev. Lett.* **90**, 127903 (2003).
30. H. Kübler, J. P. Shaffer, T. Baluktsian, R. Löw, T. Pfau, *Nat. Photonics* **4**, 112–116 (2010).
31. C. H. Bennett *et al*., *Phys. Rev. Lett.* **70**, 1895–1899 (1993).
32. H. Choi, M. Pant, S. Guha, D. Englund, *npj Quantum Inf.* **5**, 104 (2019).
33. V. Paulisch, M. Perarnau-Llobet, A. González-Tudela, J. I. Cirac, *Phys. Rev. A (Coll. Park)* **99**, 043807 (2019).
34. E. J. Davis, Z. Wang, A. H. Safavi-Naeini, M. H. Schleier-Smith, *Phys. Rev. Lett.* **121**, 123602 (2018).
35. J. P. Covey *et al*., *Phys. Rev. Appl.* **11**, 034044 (2019).
36. S. G. Menon, K. Singh, J. Borregaard, H. Bernien, *New J. Phys.* **22**, 073033 (2020).

ACKNOWLEDGMENTS

We thank C. Senko, H. Levine, D. Bluvstein, R. Riedinger, M. Bhaskar, D. Levonian, J. Borregaard, F. Reiter, S. Schwartz, J. Thompson, and A. Zibrov for useful discussions and experimental contributions. **Funding:** This work was supported by the Center for Ultracold Atoms, the National Science Foundation, Air Force Office of Scientific Research Multidisciplinary University Research Initiative, Vannevar Bush Faculty Fellowship, US Department of Energy (DOE) QSA Center (contract 7568717), and Army Research Laboratory CDQI. B.G. acknowledges support from the US Department of Defense (DOD) NDSEG. The device was fabricated at the Harvard Center for Nanoscale Systems (CNS) (NSF ECCS-1541959). **Author contributions:** T.Đ., P.S., P.L.O., and H.B. built the experimental setup, performed the measurements, and analyzed data. B.G. and I.D. assisted with experiments. All work was supervised by V.V. and M.D.L. All authors discussed the results and contributed to the manuscript. **Competing interests:** V.V. and M.D.L. are cofounders and shareholders of QuEra Computing. The other authors declare no competing interests. **Data and materials availability:** All data needed to evaluate the conclusions in the paper are present in the paper and the supplementary materials.

SUPPLEMENTARY MATERIALS

https://science.org/doi/10.1126/science.abi9917
Materials and Methods
Figs. S1 to S10
Table S1
References (*37*–*48*)

29 April 2021; accepted 29 July 2021
10.1126/science.abi9917